Electronic Supplementary Material (ESI) for Molecular BioSystems.

Supporting Information

S1. Construction of PfHGXPRT mutants W181S/F197W

The mutant, W181S was generated by quick change PCR method using a single mutagenic primer.[S1] This was performed in two steps; first an EcoRV site was introduced using pTrc99A–PfHGXPRT clone as template and 5′AGAACACCTTT**GATATC**TGGTTTTAAAGCTGAT3′ as the primer. With this mutant as the template and 5′ AGAACACCTTTG**TCGAAT**GGTTTTAAAGCTGAT3′ as the primer, EcoRV site was removed, and the mutant W181S was generated. The mutation was verified by DNA sequencing. The double mutant W181S/F197W was generated by the quick change PCR method using pTrc99A-W181S clone as the template and the primers;

5′ CAATTCCTGATCAC**TGG**GTTGTTGGTTATAGTTTAGAC 3′ and

3′ GTCTAAACTATAAC**CAA**CAACCCAGTGATCAGGAATTG 5′.

The sequences indicated in bold correspond to the introduced mutation. Following verification of mutation by DNA sequencing, the clone was expressed in the *E. coli* strain SΦ609.

S2. Purification of PfHGXPRT, F197W and W181S/F197W

SΦ609 *E. coli* cells transformed with pTrc99A construct carrying the gene for PfHGXPRT or the mutants F197W and W181S/F197W were grown in terrific broth containing 100 μg ml^{-1} of ampicillin and 25 μg ml^{-1} of streptomycin at 310 K till an optical density of 0.6 at 600 nm. Thereafter, the culture was treated with 0.1 mM isopropyl β-D thiogalactopyranoside (IPTG) in case of PfHGXPRT, 0.2 mM IPTG in case of F197W and 0.7 mM IPTG in case of W181S/F197W and, incubated at 310K for a further duration of 18 hours. Purification of

PfHGXPRT was carried out according to earlier published protocols.[S2,S3] F197W and W181S/F197W were purified using the same procedure.

S3. Solvent deuterium kinetic isotope effects (SKIE)

PfHGXPRT in 10 mM potassium phosphate, pH 7.0 was lyophilized free of water, dissolved in D_2O, and lyophilized for a second time. A control sample in H_2O was similarly lyophilized twice. Prior to use in enzyme assays, both the dried samples were dissolved appropriately in either D_2O or H_2O. The protein sample in H_2O subjected to two rounds of lyophilization did not exhibit any measurable change in activity. Xanthine phosphoribosylation activity by unactivated PfHGXPRT was monitored in 99.9% deuterated 100 mM Tris DCl, pD 7.4. Xanthine, PRPP and $MgCl_2$ were also dissolved in D_2O. Concentrations of xanthine, PRPP, free $MgCl_2$ and PfHGXPRT were fixed at 100 μM, 1 mM, 12 mM and 2.5 μM, respectively. The assay was performed by using a spectrophotometer attached to a stopped flow module (SFM 300, Biologic, France) using a cuvette of path-length 1 cm, total flow rate of 7 ml/sec and a dead time of 4.3 milliseconds. The total duration of each scan was 159.99 seconds with a sampling period of 10 milliseconds resulting in a total of 8000 data points in a single progress curve. A parallel xanthine phosphoribosylation assay was performed in H_2O at pH 7.4 by maintaining identical experimental conditions.

S4. Isothermal titration calorimetry (ITC) to determine dissociation constant for PfHGXPRT.IMP complex.

In order to estimate the dissociation constant of PfHGXPRT.IMP complex, isothermal titration calorimetry was performed using VP-ITC (Microcal, USA) calorimeter. IMP titration involved 30, 20 µl injections of 3.2 mM IMP into 169 µM PfHGXPRT. Data obtained was plotted as kcal of heat released per mole of IMP against the molar ratio [PfHGXPRT]:[IMP] and fit to one binding site model (equation i) using ORIGIN software and Hill's equation (equation ii) for cooperativity using Graph Pad Prism (Version 5, San Diego, California).

$$Y = (Y_{max}*[R]) / (K_d+[R])\text{……..(i)}$$

$$Y = Y_{max}*[R]^h/(K' + [R]^h)\text{……..(ii)}$$

In both equations, Y and R represent kcal of heat released and the value of the ratio [PfHGXPRT]/[IMP], respectively. In equation (i), K_d is the dissociation constant for PfHGXPRT.IMP complex and Y_{max} is the maximum value of heat released. In equation (ii), 'h' represents Hill's coefficient and K′ is the modified dissociation constant which is a function of several interaction parameters. It is given by $K_d^h(a^{h-1}.b^{h-2}.c^{h-3}\text{……}z^1)$, wherein a, b, c……z indicate interaction factors that represent the magnitude by which the K_d value gets modified as a result of cooperativity in ligand binding.

S5. Energetics of the conformational change of isolated Leu 76 – Lys 77 dipeptide

To understand the energetics of this bond rotation in gas phase, the Leu-Lys dipeptide was isolated from the protein backbone. Gas phase quantum calculations at B3LYP/6-31g level of theory were carried out using Gaussian software.[S4] The two termini of the dipeptide were truncated by adding two -CH_3 groups. The dihedral angle, ω (along the amide bond) was scanned from 0^o (cis) to 180^o (trans) using the relaxed redundant scan procedure as implemented in Gaussian 09.[S4] The cis-to-trans rotational barrier was found to be 19 kcal/mol with the trans form of dipeptide stable by 8 kcal/mol (Figure S14a).

Subsequently, the isolated dipeptide was solvated in a cubic simulation box filled with 1502 SPC/E water molecules. Choosing the dihedral angle (ω) as the collective variable (COLVAR), a Well Tempered Metadynamics (WTM) simulation of length 50 ns was performed using the Amber force field with the reoptimized dihedral parameter[S5], to estimate the free energy change for the rotation around the amide bond of the dipeptide. Plumed-2.0.1 patched with Gromacs-4.5.5 was used to perform the WTM simulations. A cis to trans rotational barrier and cis-trans energy difference of 17 kcal/mol and 4 kcal/mol (favoring the trans), respectively were estimated. The free energy profile is displayed in Figure S14b. Thus, quantum chemical calculations in gas phase of the dipeptide as well as Potential of Mean Force (PMF) calculations of the same in water at 300K provide convincing evidence for the stability of the trans conformation of the Leu-Lys dipeptide.

S6. Ligand-free PfHGXRT with the Leu-Lys dipeptide in cis and trans conformations: Structural comparison

In this section, we compare the structures of ligand-free PfHGXPRT with the dipeptide either in cis or trans conformations. Both of them were obtained from computer simulations, as described in the main manuscript.

The position of loop II in both the protein structures was found to be nearly same (Figure 9 of the main manuscript). In the cis conformation, Lys 77 side chain is oriented away from the active site of the protein. However, in the trans conformation, the side chain moves down towards the cavity and is seen to participate in the following interactions: (a) with the –COO- group in the side chain of Glu 144 through the formation of a salt bridge between the $–NH_3^+$ group of the side chain and the –COO- of the Glu reside and (b) with the backbone –C=O of the Ile 146 (Figures S16 & S17, movie 2). Similar interaction motifs are observed in the human HGPRT protein as well. In the ligand-bound (1BZY) enzyme, the side chain of Lys 68 is pointed outward and interacts with the side chain of Asp 97 and backbone –C=O of Val 96, while the same interacts with $–COO^-$ of Asp 133 and backbone –C=O of Ile 135 in the free protein (1Z7G).

Additionally, a comparison of the Ramachandran plots (Figure S18) of the ligand-free PfHGXRT (obtained from the free energy run) and the human ligand-free enzyme with the trans dipeptide reveal much structural similarities between them. These comparisons allow us to believe that the protein obtained from the WTM simulation can serve as a model for the apo *Plasmodium falciparum* HGXPRT.

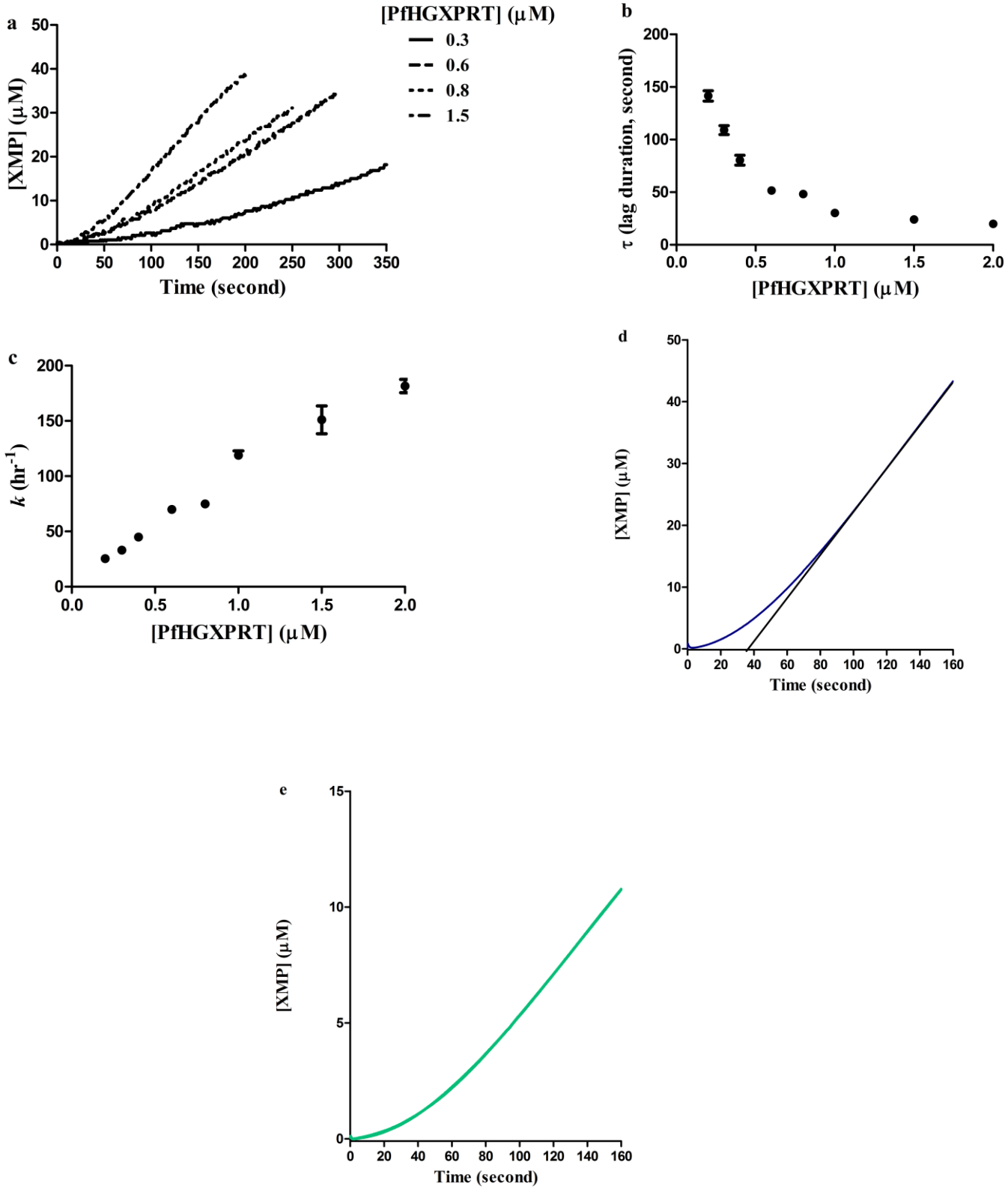
a
[PfHGXPRT] (μM)
0.3
0.6
0.8
1.5
[XMP] (μM)
Time (second)
b
τ (lag duration, second)
[PfHGXPRT] (μM)
c
k (hr-1)
[PfHGXPRT] (μM)
d
[XMP] (μM)
Time (second)
e
[XMP] (μM)
Time (second)

Figure S1. Hysteretic behavior of unactivated PfHGXPRT. a) Representative progress curves of xanthine phosphoribosylation (in potassium phosphate) showing decrease in duration of lag phase upon increase in concentration of PfHGXPRT. b) Inverse relation between lag durations in panel a and concentration of PfHGXPRT. Saturation in lag duration occurs at 1 μM concentration of enzyme. c) Increase in rate constant for switch from lag phase to steady state phase in xanthine phosphoribosylation reaction (in potassium phosphate) with increase in concentration of PfHGXPRT. The rate constants were calculated from the reciprocal of lag durations in the progress curves. These rate constants represent the events of PRPP binding, oligomerization and conformational switch of L76-K77 dipeptide from trans to cis conformation. d) Lag duration in xanthine phosphoribosylation reaction (in potassium phosphate) estimated using a stopped flow spectrophotometer at PfHGXPRT concentration of 2.5 μM. This concentration corresponds to the plateau in panel b. The lag duration estimated from the progress curve was 37.1 seconds and the corresponding rate constant for approach to steady state is 97 hr^{-1}. e) Lag duration in xanthine phosphoribosylation reaction (in Tris HCl) estimated using a stopped flow spectrophotometer at PfHGXPRT concentration of 2.5 μM. This concentration corresponds to the plateau in Figure 2, panel b. The lag duration estimated from the progress curve was 40.8 seconds and the corresponding rate constant for approach to steady state is 88 hr^{-1}. For assays in potassium phosphate, xanthine and PRPP concentrations were fixed at 100 μM and 1 mM, respectively. When Tris HCl was used as the assay buffer (panel e), xanthine concentration was same, but PRPP concentration was fixed at 3 mM.

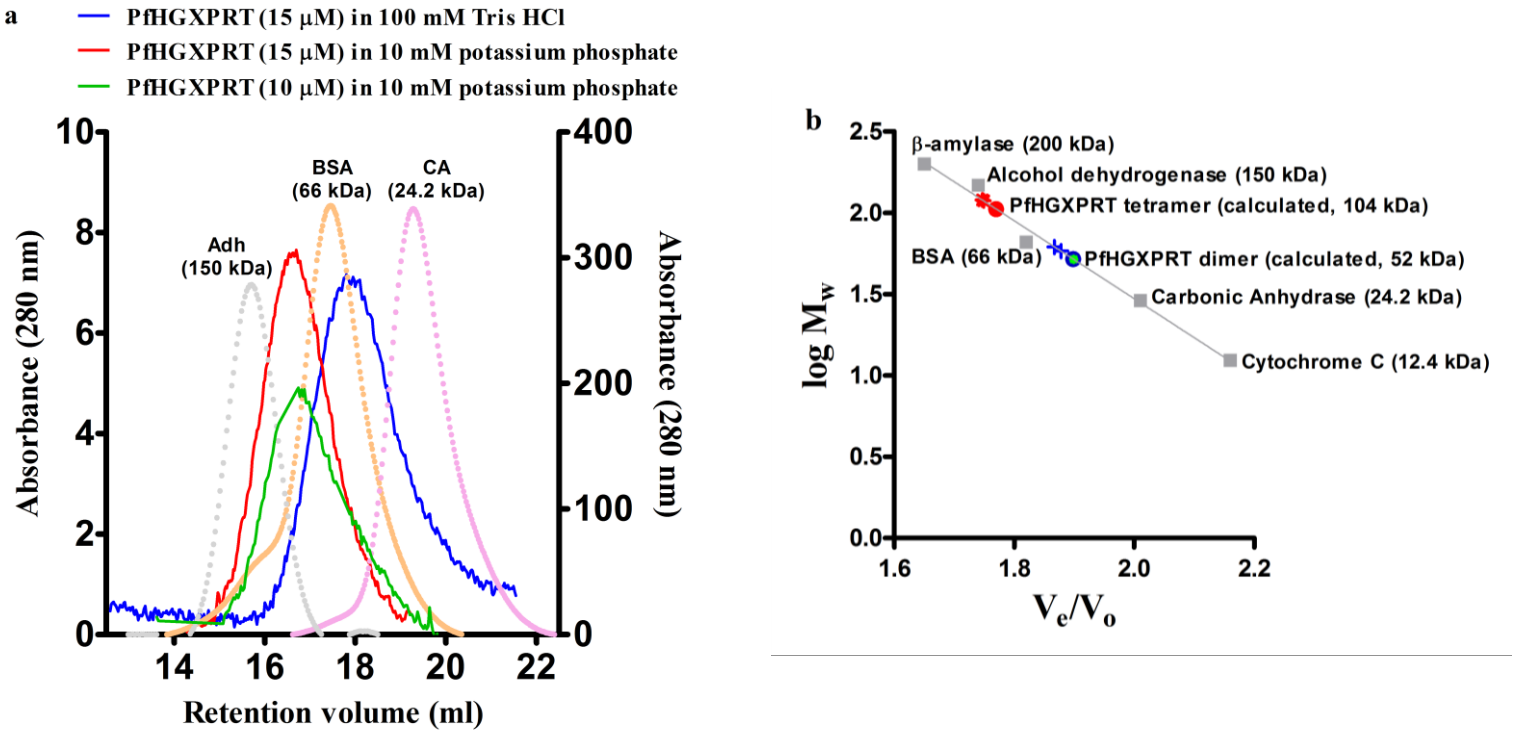

Figure S2. Oligomeric state of PfHGXPRT in Tris HCl and phosphate buffers as examined by analytical size-exclusion chromatography. a) Chromatograms of PfHGXPRT in 10 mM potassium phosphate (red, green) and 100 mM Tris HCl (blue). The absorbance values for the protein molecular weight standards (alcohol dehydrogenase (Adh) in grey, bovine serum albumin (BSA) in orange and carbonic anhydrase (CA) in pink) are on the right Y-axis and for PfHGXPRT on the left Y-axis. The molecular weights of PfHGXPRT obtained in 10 mM potassium phosphate and 100 mM Tris HCl are 118 kDa and 58 kDa, respectively where the former corresponds to tetramer and the latter dimer. The volume of PfHGXPRT injected in all cases was 100 µl while the concentration of the enzyme in the injected solution was 15 µM (red) and 10 µM in phosphate (green) and, 15 µM in Tris (blue). The concentration of PfHGXPRT under the peak, after correction for dilution on the column is, 0.3 µM (red), 0.2 µM (green) and 0.4 µM (blue). It should be noted that despite the heavy dilution, the elution volumes at the peak are distinct in Tris and phosphate and correspond to dimers and tetramers, respectively. However, presence of dimers in phosphate buffer at these low concentrations of protein cannot be ruled out. Direct injection of 1-2 µM

enzyme would result in lowering of concentration to 0.07-0.13 μM upon dilution on the column and thus preclude the visualization of the peak. b) Calibration curve of protein molecular weight standards. The solid circles in red and blue are the calculated molecular weights of PfHGXPRT tetramer (104 kDa) and dimer (52 kDa), respectively. The points represented by * and + correspond to the experimental data points of V_e/V_o for PfHGXPRT in 10 mM potassium phosphate and 100 mM Tris HCl, respectively. The point represented by * corresponds to the experimental data point of V_e/V_o for PfHGXPRT in 10 mM Tris HCl. M_w and V_e correspond to the molecular weight and retention volumes of the proteins, respectively. V_o is the void volume of the column that was measured using blue dextran (2000 kDa). All the chromatographic runs were performed using Superdex S-200 column (30 cm x 1cm) attached to an ÄKTA Basic HPLC. The flow rate was fixed at 0.5 ml/min and absorbance of the eluate was monitored at 280 nm.

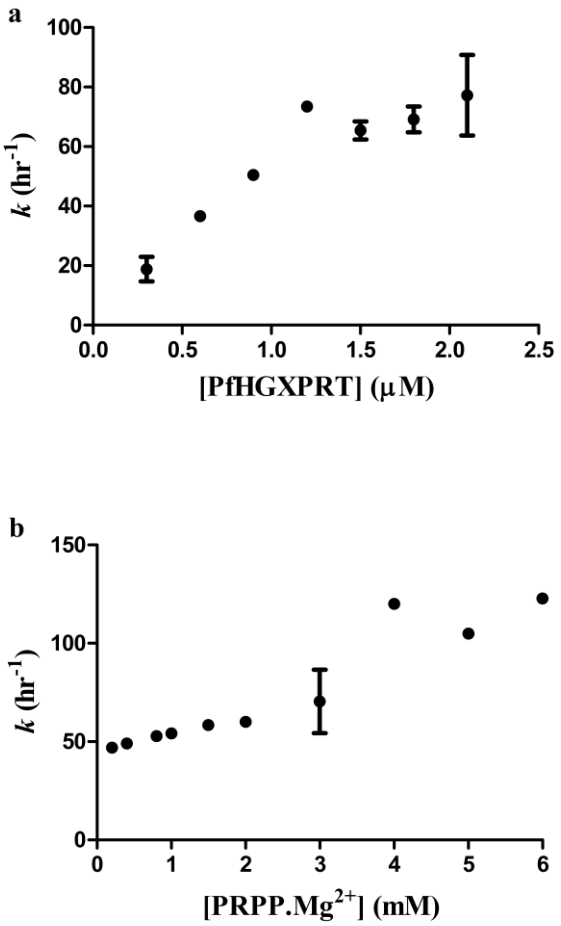

Figure S3. Increase in magnitude of rate constant for approach from lag phase to steady state phase upon a) increase in concentration of PfHGXPRT b) increase in concentration of PRPP. Assays were performed in 100 mM Tris HCl, pH 7.4. The rate constants have been estimated by reciprocal of lag duration in plots shown in figures 2a and 2b. Xanthine and PRPP concentrations were fixed at 200 µM and 3 mM, respectively. Concentration of free $MgCl_2$ was maintained at 12 mM. The plots are representative of 3-5 replicate experiments.

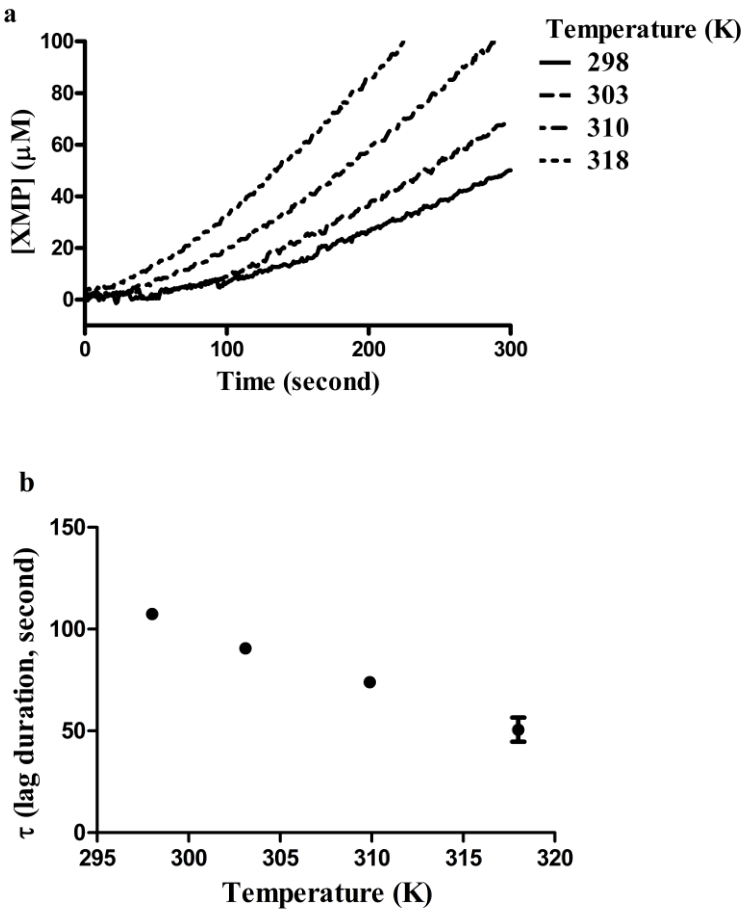

Figure S4. Temperature dependence of lag duration in xanthine phosphoribosylation by unactivated PfHGXPRT. a) Representative progress curves of xanthine phosphoribosylation showing decrease in the duration of lag phase upon increase in temperature. b) Inverse relation between lag duration and temperature. Xanthine and PRPP concentrations were maintained at 200 μM and 3 mM, respectively. Concentration of free $MgCl_2$ was fixed at 12 mM. The assays were performed in 100 mM Tris HCl, pH 7.4.

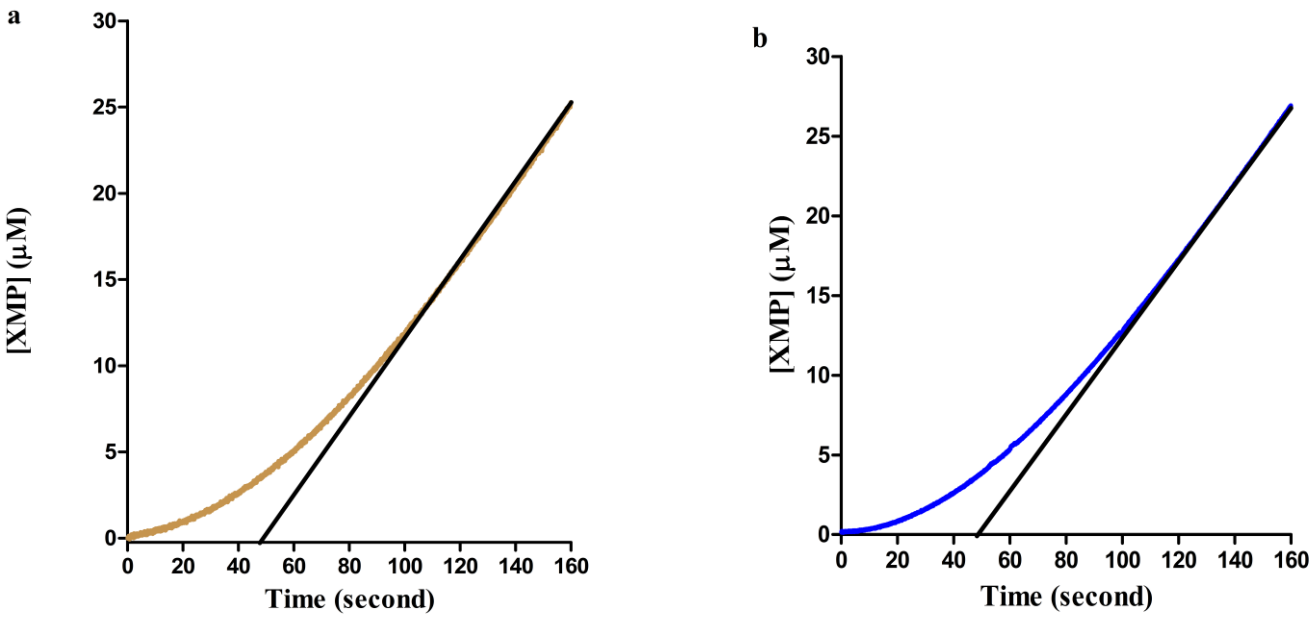

Figure S5. Progress curves of xanthine phosphoribosylation activity by unactivated PfHGXPRT performed in a) D_2O and b) H_2O. Both samples were lyophilized twice and resuspended in D_2O/H_2O. The lag duration estimated in the two cases are 48.7 and 47.7 seconds, respectively. The reciprocal of the lag durations result in a rate constant of 120 hr^{-1} for approach to steady state phase. Xanthine, PRPP, free $MgCl_2$ and unactivated PfHGXPRT in both cases were maintained at 100 μM, 1 mM, 12 mM and 2.5 μM, respectively. The assays were performed in 100 mM Tris DCl, pD 7.4 and 100 mM Tris HCl, pH 7.4, respectively.

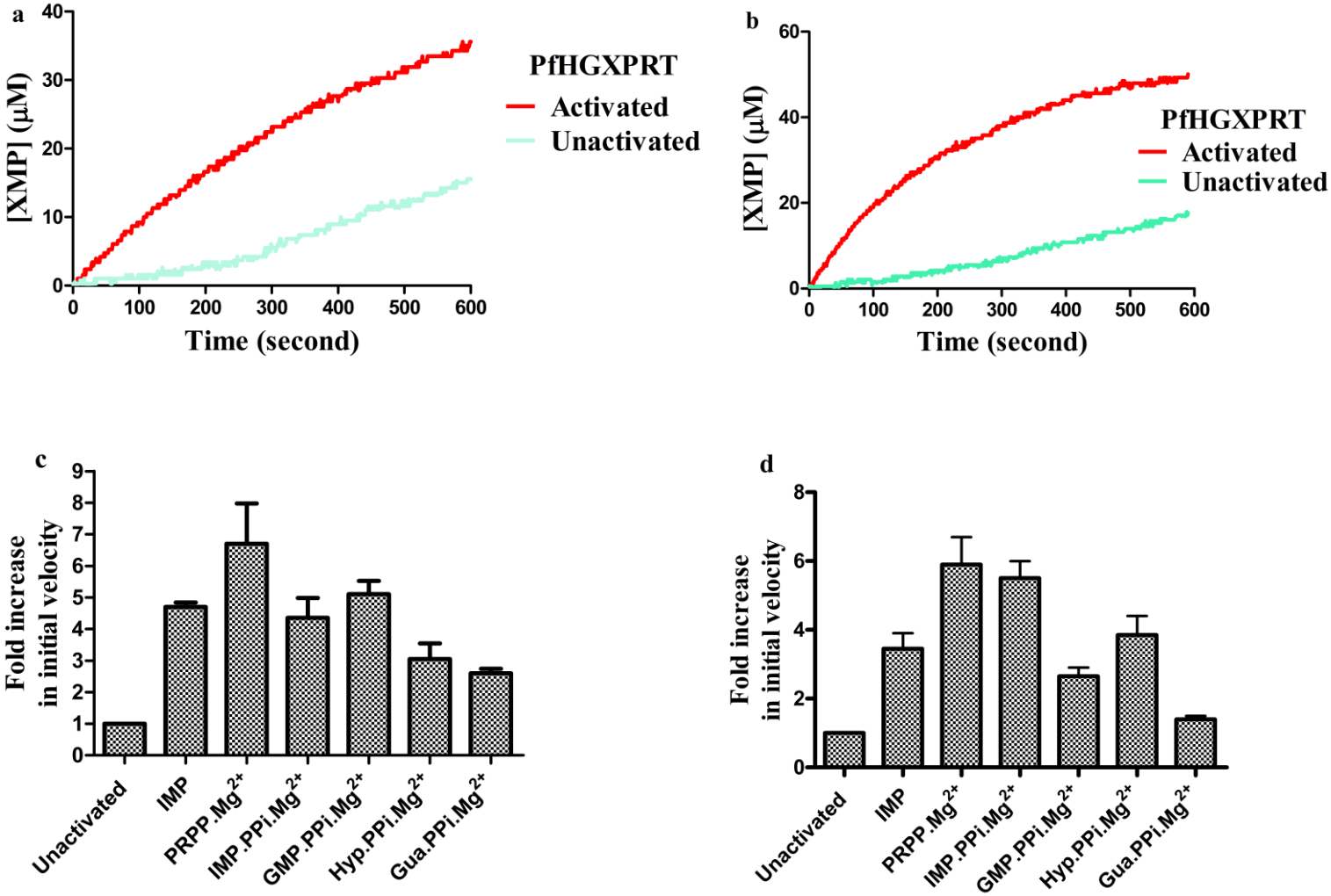

Figure S6. Activation of PfHGXPRT with different ligand/s. a) Representative progress curves of xanthine phosphoribosylation by unactivated and activated PfHGXPRT. For activation, 30 μM PfHGXPRT was pre-incubated with ligand/s in 10 mM potassium phosphate, pH 7.0 for 3 hours at 273 K. Unactivated PfHGXPRT was used as control wherein, PfHGXPRT at the same concentration was pre-incubated under the same conditions without ligand/s. The assay was performed in 10 mM potassium phosphate, pH 7.4. b) Representative progress curves of xanthine phosphoribosylation by unactivated and activated PfHGXPRT, when both activation and xanthine phosphoribosylation assay were performed in 100 mM Tris HCl, pH 7.4. Activation was performed at the same concentration of PfHGXPRT (as mentioned in panel a), in 100 mM Tris HCl, pH 7.4. Unactivated PfHGXPRT was pre-incubated at 273K

in Tris HCl buffer without ligand/s. c) Comparison of magnitudes of activation in presence of different ligand/s with respect to the unactivated state under the conditions given for panel a. d) Comparison of magnitudes of activation in presence of different ligand/s with respect to the unactivated state under the conditions given for panel b. [IMP]/[GMP] carried over to the reaction mix were 0.48 and 0.96 µM, respectively for panels a and b. In all panels, xanthine, PRPP and free $MgCl_2$ concentrations were fixed at 100 µM, 1 mM and 12 mM, respectively. Enzyme concentrations in the assay mix were 0.2 and 0.3 µM, respectively for panels a and b. These enzyme concentrations were achieved without any prior dilution. The plots are representative of 3-5 replicate experiments.

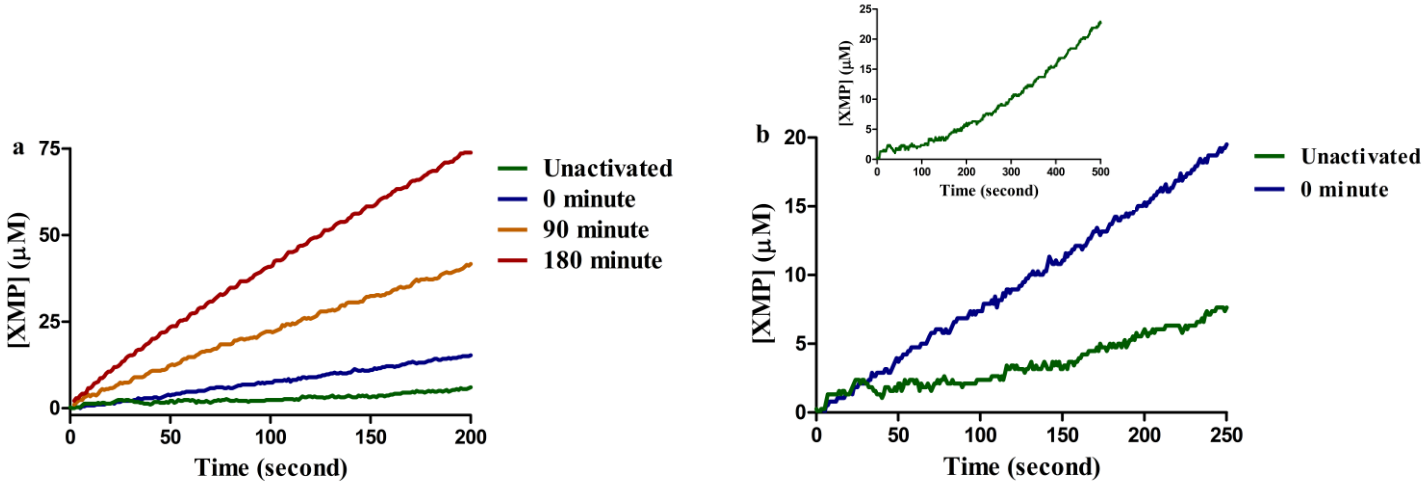

Figure S7. Time dependence of activation in PfHGXPRT shows that lag vanishes at zero-time while activation is slow. a) Progress curves of xanthine phosphoribosylation activity by $PRPP.Mg^{2+}$ activated PfHGXPRT at different time durations of activation. b) Progress curves of xanthine phosphoribosylation activity by unactivated PfHGXPRT and PfHGXPRT immediately after pre-mixing with $PRPP.Mg^{2+}$ (0 minute activation). It should be noted that the activity of PfHGXPRT remains low at 0 minute of pre-incubation with $PRPP.Mg^{2+}$, but the lag disappears completely. The specific activities of unactivated enzyme and after 0 minute of pre-incubation are 0.5 and 0.7 µmole.mg^{-1}.min^{-1}, respectively. In case of the unactivated enzyme, the v_o values were taken from the initial steady state phase of the progress curves

after excluding the lag. The duration of the lag phase in each progress curve had been estimated by drawing a tangent from the steady state phase to the X-axis. The complete time course for xanthine phosphoribosylation by unactivated PfHGXPRT is represented as an inset to panel b. The activation mix consisting of 30 μM enzyme and 1 mM PRPP.Mg^{2+} was incubated at 273K in 10 mM potassium phosphate, pH 7.0, for different time durations and used for activity measurements. Unactivated PfHGXPRT was used as control where, PfHGXPRT at the same concentration was pre-incubated under the same conditions without PRPP.Mg^{2+}. Concentrations of xanthine, PRPP and PfHGXPRT in all assays were fixed at 200 μM, 1 mM and 0.2 μM, respectively.

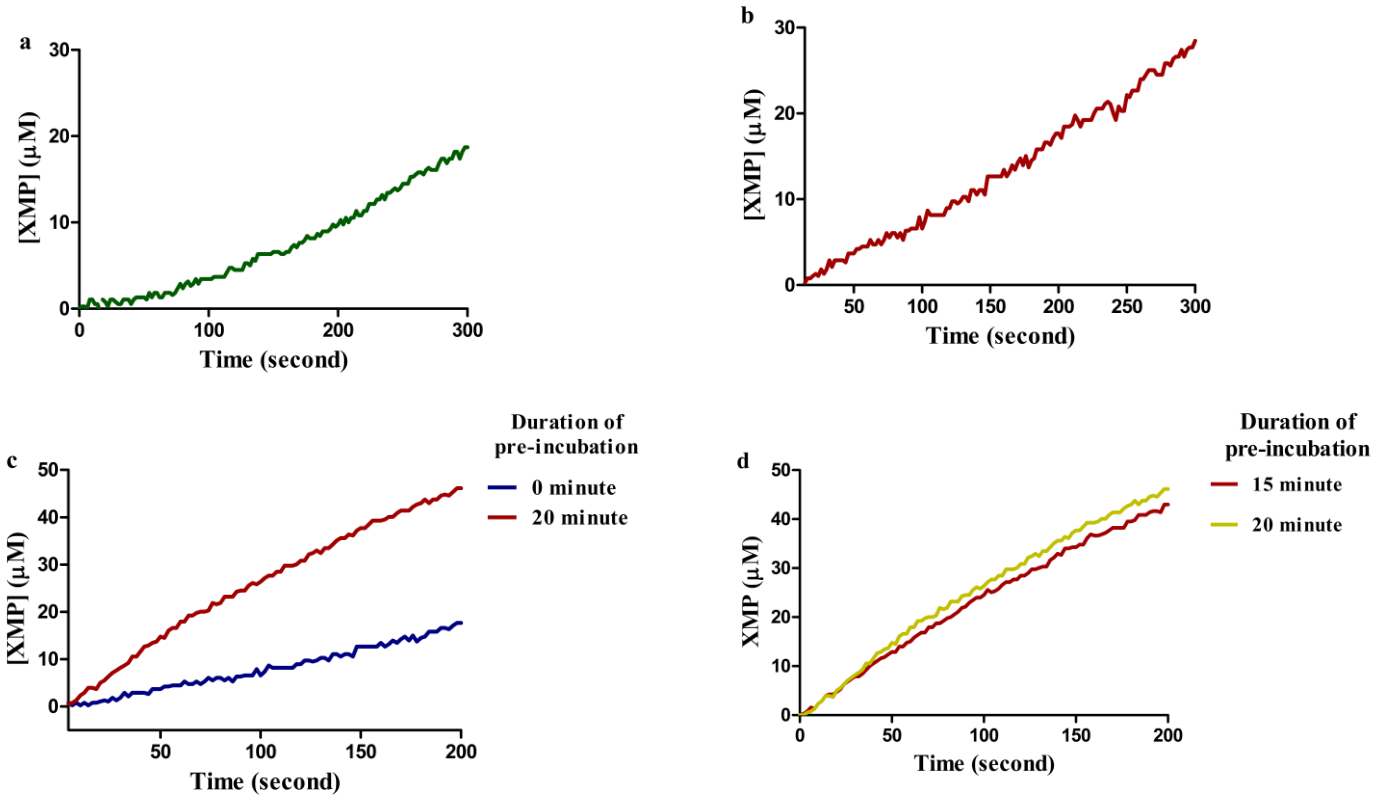

Figure S8. Time dependence of activation when 0.4 μM PfHGXPRT is activated with 1 mM PRPP and 12 mM $MgCl_2$ at 296K in 10 mM potassium phosphate, pH 7.0. a) The lag phase exists in the xanthine phosphoribosylation activity by unactivated PfHGXPRT. Unactivated PfHGXPRT was used as control where, PfHGXPRT at the same concentration was pre-incubated under the same conditions without $PRPP.Mg^{2+}$. b) The lag phase is absent when xanthine phosphoribosylation activity is measured at '0 minute' of pre-incubation. The specific activity of the unactivated enzyme is 0.3 $\mu mole.mg^{-1}.min^{-1}$ and that measured at 0 minute of pre-incubation is 0.4 $\mu mole.mg^{-1}.min^{-1}$. The v_o value for the unactivated PfHGXPRT in panel a was estimated in the same manner as mentioned in Figure S7. c) Overlay of the time courses of xanthine phosphoribosylation activity at 0 and 20 minutes of pre-incubation. d) Overlay of the time courses of xanthine phosphoribosylation activity at 15 and 20 minutes of pre-incubation. Complete activation is achieved within a time duration of 15 minutes. The initial slope of the time course at time duration of 15 and 20 minutes of pre-incubation are 3-fold higher than the initial slope of the time course at 0 minute of pre-incubation. The initial slopes of the of the progress curves at 15 minutes and 20 minutes time duration of pre-incubation are equal.

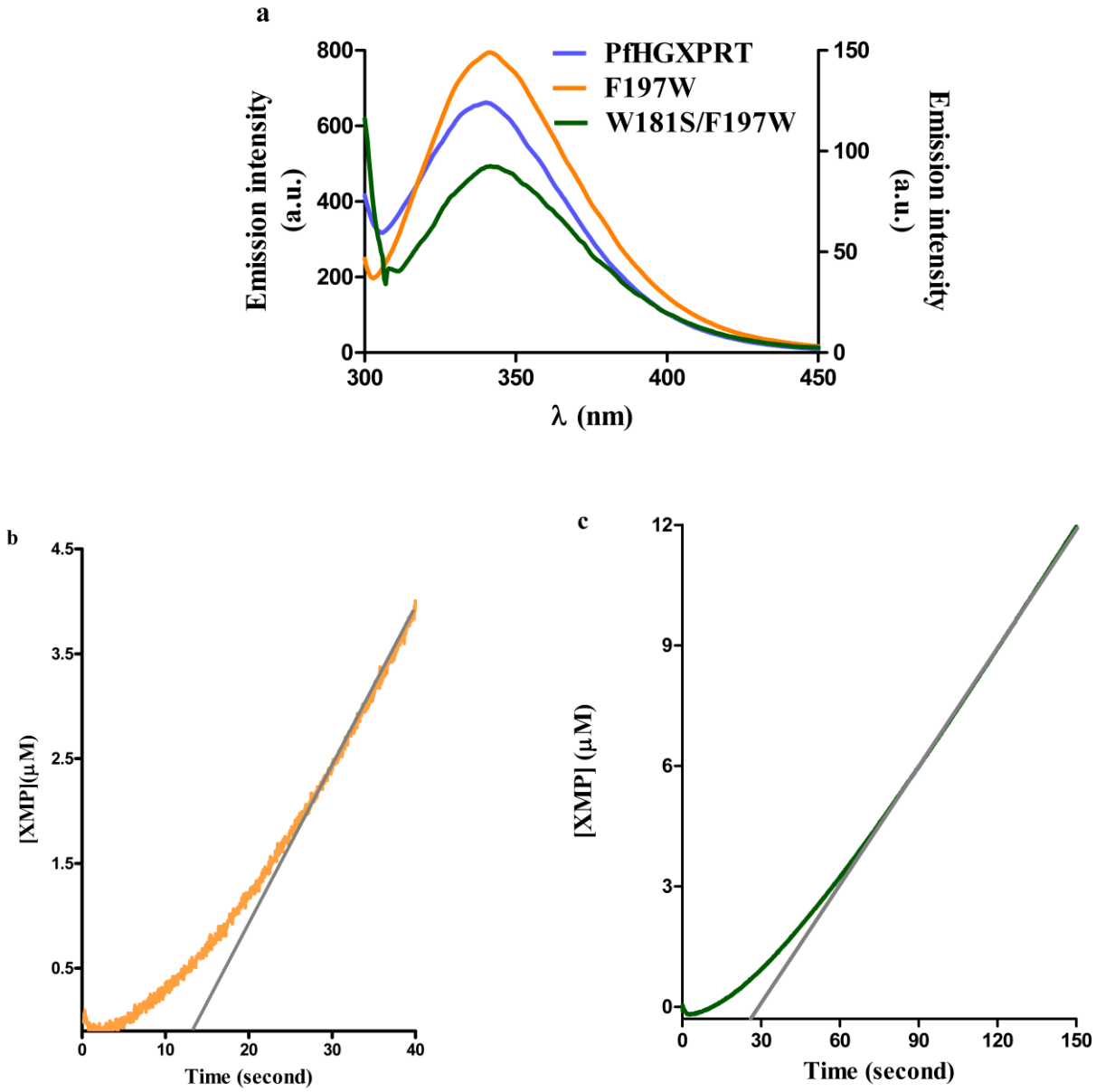

Figure S9. Biochemical properties of PfHGXPRT mutants F197W and W181S/F197W. a) Fluorescence emission spectra of PfHGXPRT, F197W and W181S/F197W in 10 mM potassium phosphate, pH 7.0. Wavelength for excitation was fixed at 295 nm. The emission intensity values of PfHGXPRT and F197W are represented on the left Y-axis in arbitrary units (a.u.). The emission intensity values for W181S/F197W have been represented on the right Y-axis in arbitrary units (a.u.). b) Xanthine

phosphoribosylation by unactivated F197W monitored using a stopped flow spectrophotometer. The lag duration estimated by extrapolation of the steady state phase in the progress curve to the X-axis is 13.3 seconds. Concentration of F197W was maintained at 0.8 μM. c) Xanthine phosphoribosylation by unactivated W181S/F197W monitored using a stopped flow spectrophotometer. The lag duration estimated by extrapolation of the steady state phase in the progress curve to the X-axis is 27 seconds. Concentration of W181S/F197W was maintained at 1.2 μM.

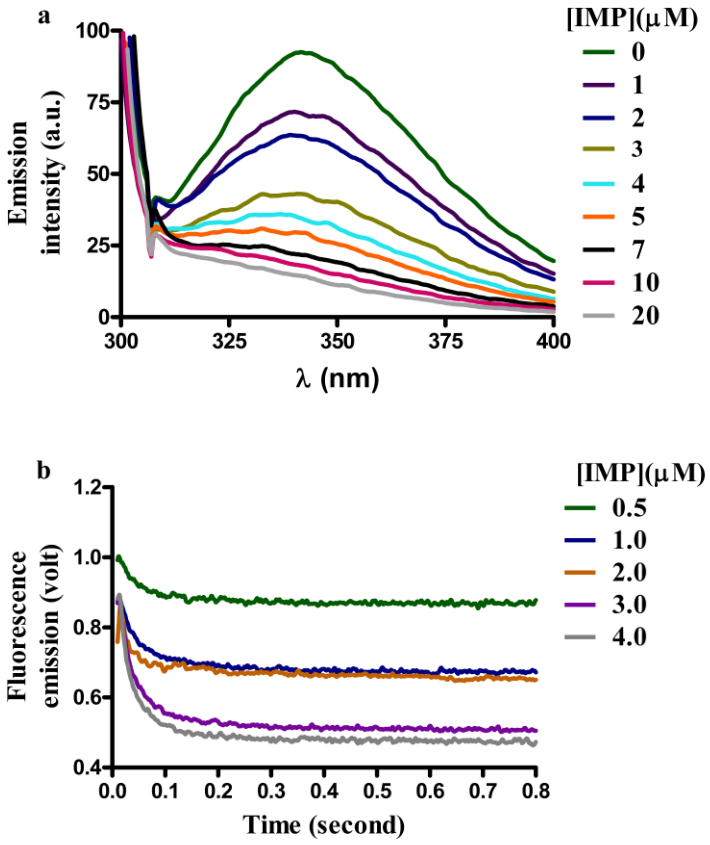

Figure S10. Quenching of tryptophan fluorescence emission of W181S/F197W upon increase in IMP concentration in 10 mM potassium phosphate, pH 7.0. a) Representative fluorescence emission spectra of W181S/F197W at different concentrations of IMP under steady state conditions. Concentration of W181S/F197W was fixed at 5μM. IMP concentration was varied from 0.5 μM to 20 μM. Fluorescence

emission intensity values are represented in arbitrary units (a.u.). b) Progress curves from stopped flow spectrophotometer representing the decrease of tryptophan fluorescence emission intensity with time upon IMP binding to the W181S/F197W. Excitation wavelength was fixed at 295 nm and emission was monitored using 320 nm cut-off filter. Each curve was an average of 10-15 scans. Concentration of the enzyme in this case was fixed at 3 µM and IMP concentration was varied from 0.5 µM to 4 µM. Fluorescence emission intensity values are represented in volts in this experiment.

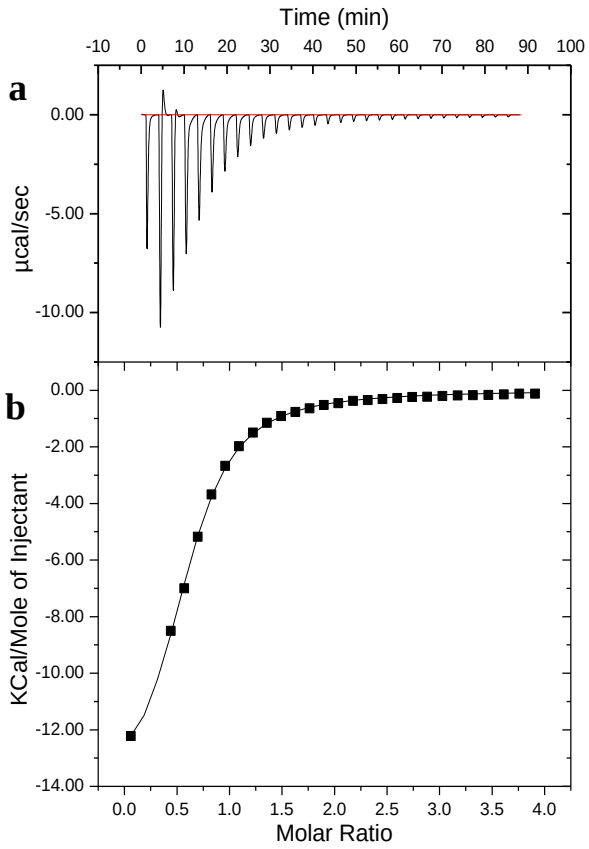

Figure S11. Estimation of dissociation constant of PfHGXPRT.IMP complex using isothermal titration calorimetry. a) Thermogram representing magnitude of heat change when IMP was titrated against PfHGXPRT. b) Magnitude of heat released (in kcal) per mole of IMP plotted against the molar ratio [PfHGXPRT]/[IMP]. The equation for one binding site was used in order to estimate the dissociation constant for PfHGXPRT.IMP complex. Comparative fitting of the data from ITC to two-site binding

model (equation i of section S4 of SI) and to Hill's equation (equation ii of section S4 of SI) yielded poor statistical parameters and ruled out cooperativity in IMP binding.

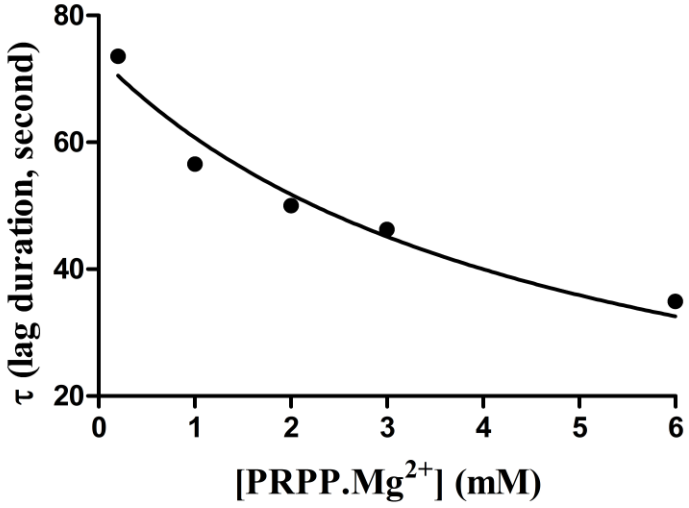

Figure S12. Lag duration (τ) plotted against concentration of PRPP.Mg^{2+}, in order to estimate the values of K_m and k_{cat}/K_m from the equation; $\tau = 1/\{k_1*([PRPP]+K_m)\}$.[S6] Here k_1 represents k_{cat}/K_m for PRPP in the lag phase that corresponds to the inactive state of PfHGXPRT and τ represents lag duration at each concentration of PRPP. Xanthine phosphoribosylation was monitored with 1 μM of unactivated PfHGXPRT using a stopped flow spectrophotometer. The assays were performed using 100 mM Tris HCl, pH 7.4 at 296K. Concentration of PRPP was varied at 0.2, 1.0, 2.0, 3.0, and 6.0 mM. Xanthine concentration was fixed at 100 μM and concentration of free $MgCl_2$ was maintained at 12 mM. Total duration of each scan was 159.9 seconds at PRPP concentrations of 0.2, 1.0, 2.0, and 3.0 mM. At PRPP concentration of 6.0 mM total duration of the scan was 79.9 seconds. The dead time was maintained at 4.3 milliseconds for every assay.

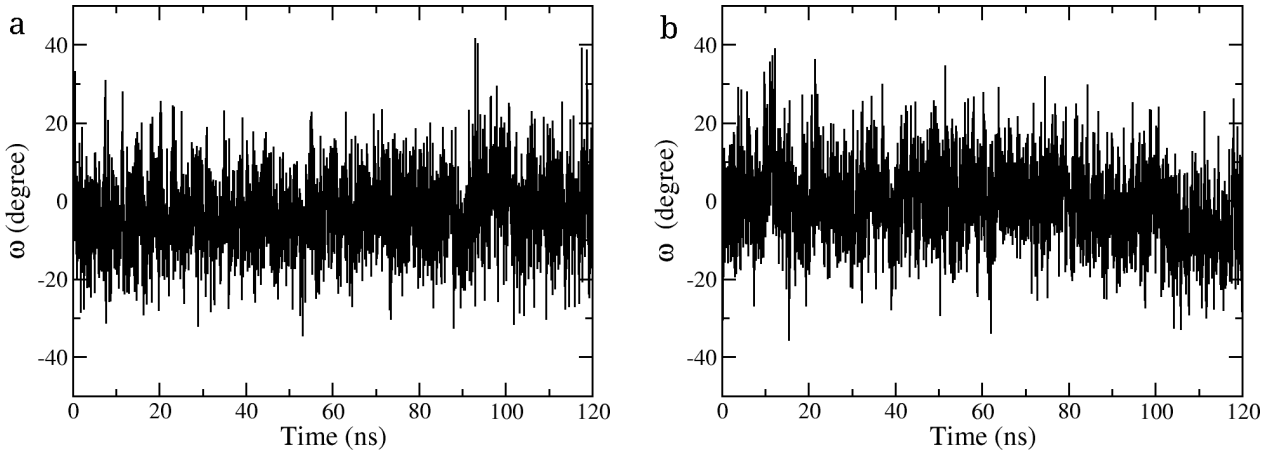

Figure S13. Dihedral angle (ω) of the Leu 76-Lys 77 dipeptide (Cα-C-N-Cα) in the (a) free and (b) ligand-bound PfHGXPRT (1CJB) as a function of time, obtained from unbiased MD simulations.

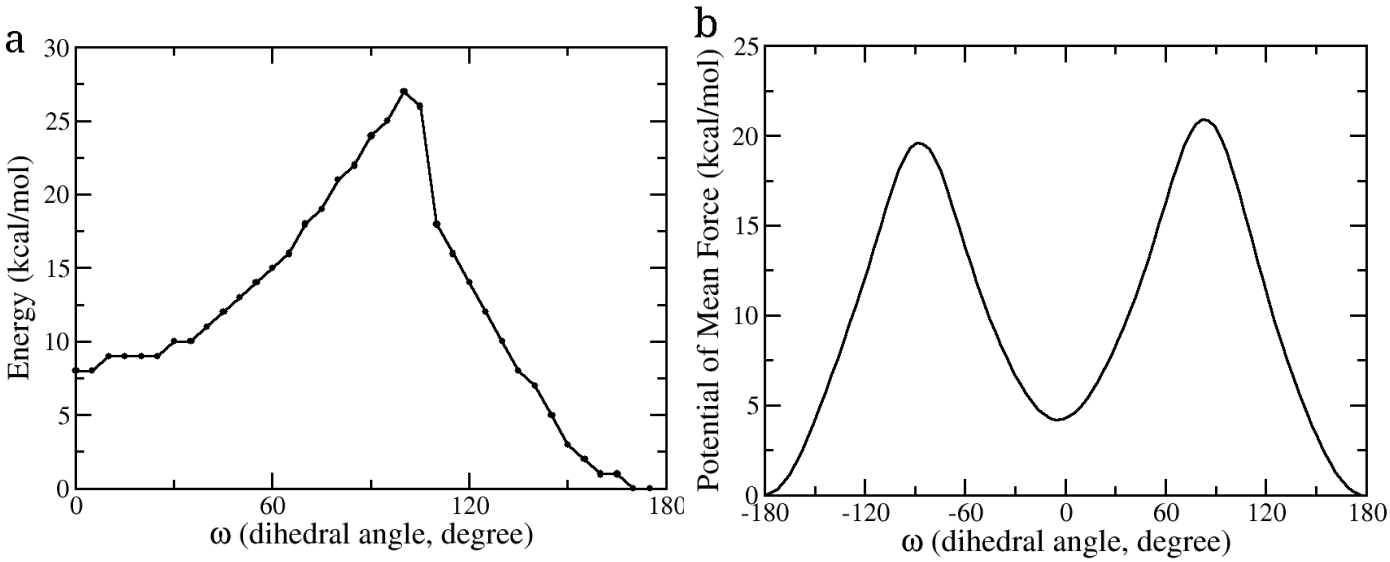

Figure S14. a) Energy profile of the Leu-Lys dipeptide in gas phase as a function of the dihedral angle (ω) calculated at B3LYP/6-31g level of theory b) Free energy profile for the conformational change of the isolated dipeptide solvated in water, calculated at 300K using AMBER94/SPCE force fields.

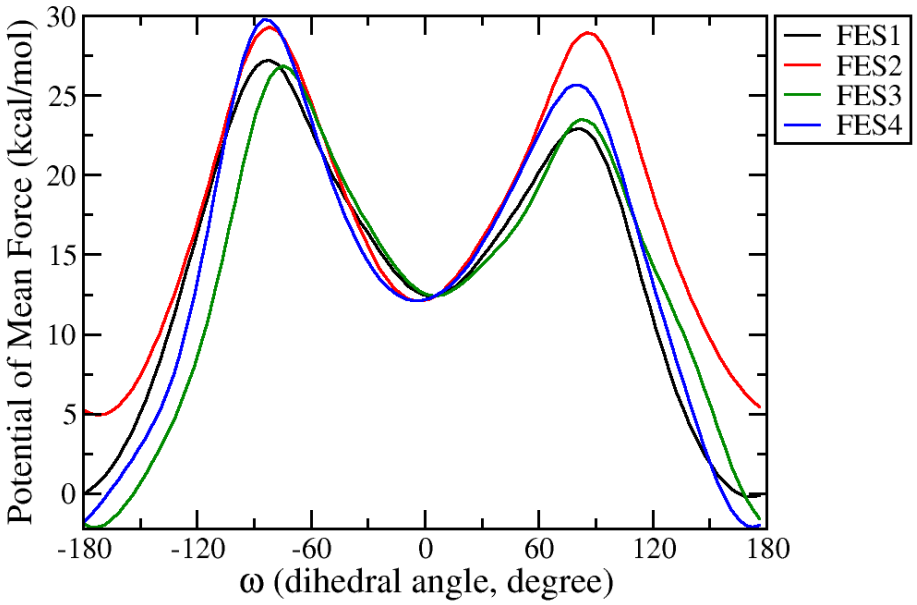

Figure S15. Free energy profiles obtained from four different WTM simulations for the rotation about the Leu-Lys peptide bond in the ligand-free PfHGXPRT enzyme in water at 300K.

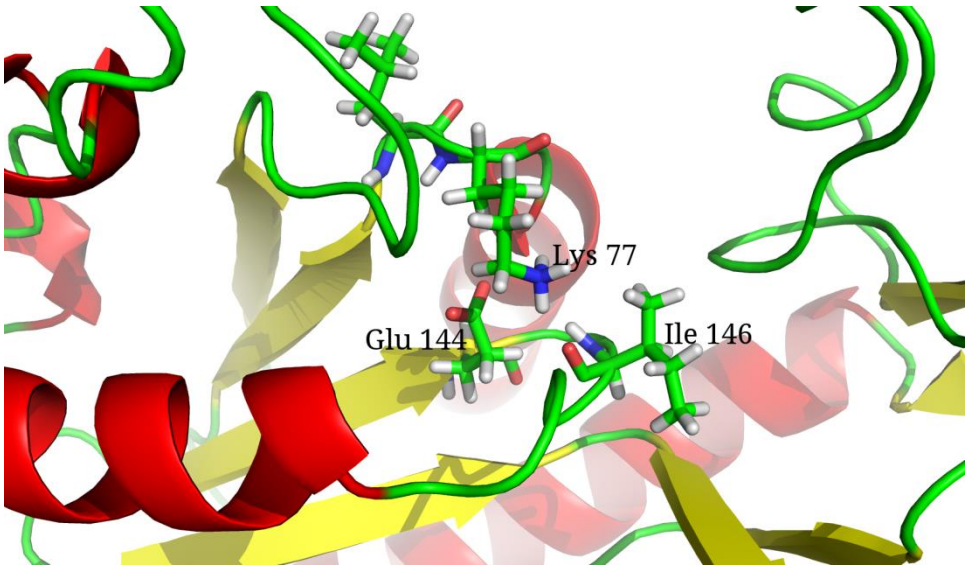

Figure S16. Interactions between side chains of Lys 77 with Glu 144 and Ile 146 in the ligand-free PfHGXPRT in trans conformation of the dipeptide, obtained from WTM run. The color coding for secondary structures is red, yellow and green for helices, β-strands and loops, respectively. The distance between the nitrogen atom (Nξ) of the Lys 77 side chain and the central carbon atom Cδ of the Glu 144 side chain is plotted against the dihedral angle (ω) to check if they are correlated. The data is shown in Figure S16. A clear correlation between the Lys side chain orientation and the dipeptide dihedral angle (ω) is observed, indicating that in the trans conformation of the dipeptide, the Lys 77 side chain moves down and is oriented towards the Glu 144 residue; however, in its cis conformation, the Lys77 side chain is far from Glu 144. During the course of the WTM runs, the reorientation of this side chain was observed, which reflects the efficiency of the configurational sampling.

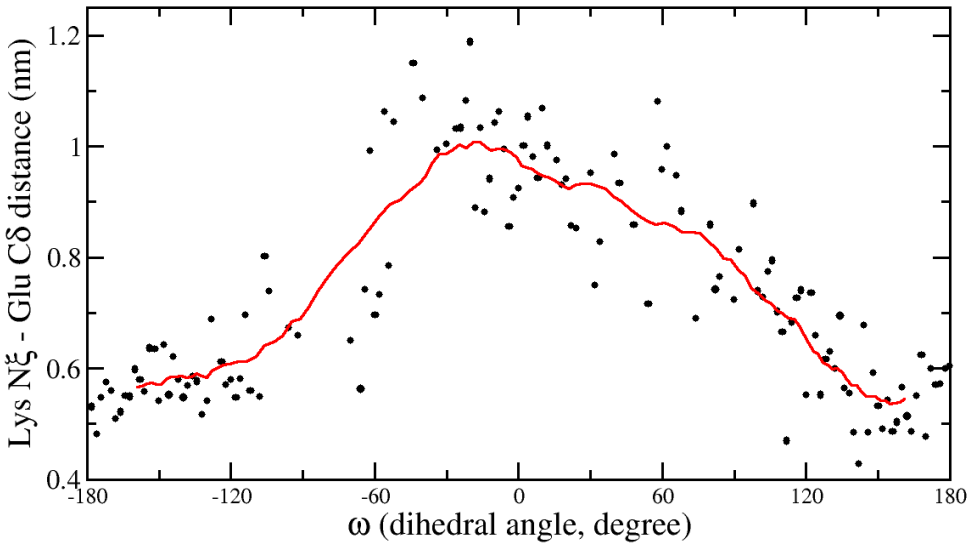

Figure S17. Distance between the nitrogen atom (Nξ) of Lys 77 side chain and the carbon atom (Cδ) of Glu 144 side chain versus the dipeptide omega dihedral angle (Cα-C-N-Cα). The data (black dots) is averaged over all the well tempered metadynamics simulation trajectories. The red curve is obtained as the running average of the black dots and is shown as an aid to the eye.

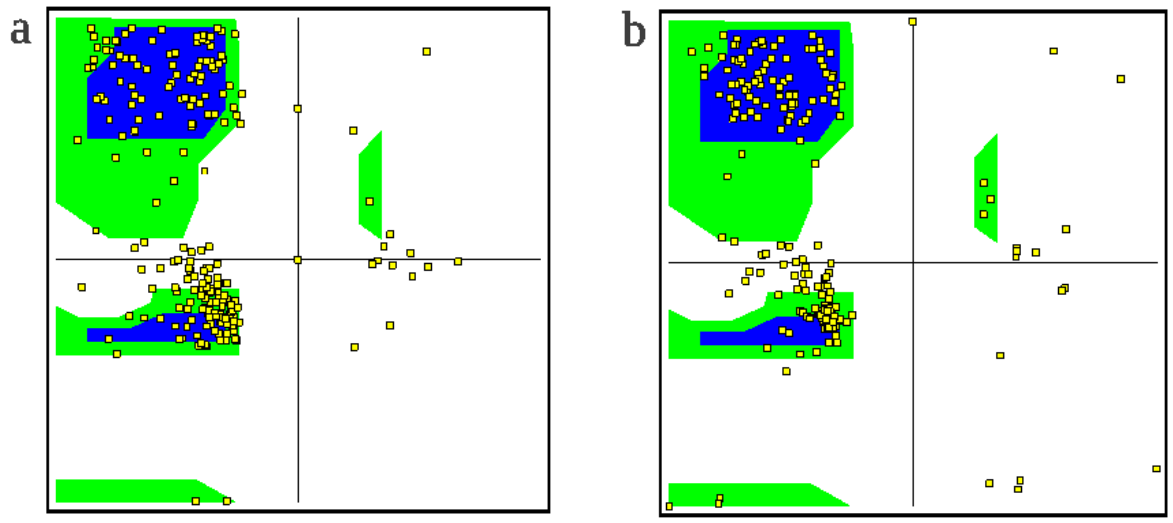

Figure S18. Ramachandran plots of (a) Free PfHGXPRT configuration arbitrarily chosen from one of the WTM simulation trajectory. (b) Free Human-HGPRT (1Z7G); the missing loop (residues 103-112) has been added by FALC Loop Modeling server.[S7]

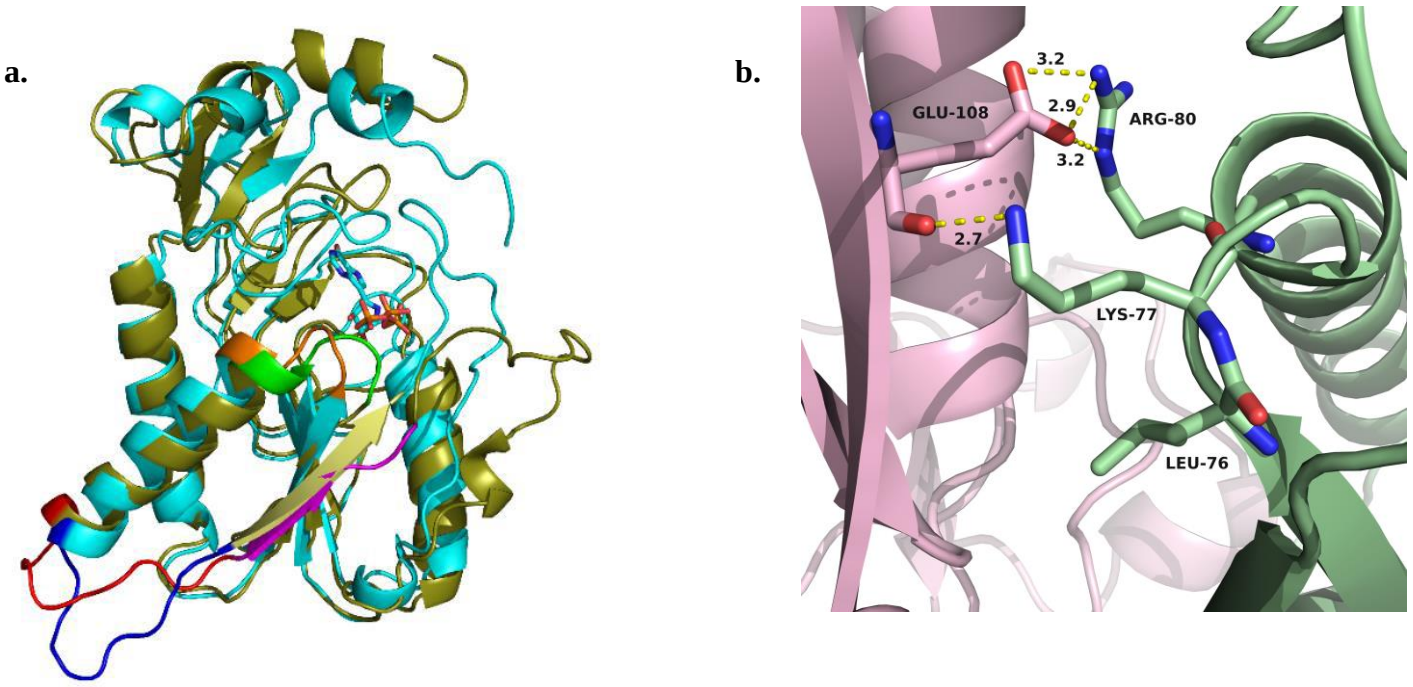

Figure S19. Conformational changes in PfHGXPRT upon trans to cis isomerization of Leu76-Lys77 peptide bond. a) Overlay of the apo, trans structure of PfHGXPRT (olive) (obtained from the simulation trajectory) and the ligand-bound cis structure of PfHGXPRT (cyan). The figure shows conformational changes in active site loop I (colored in green and orange in trans and cis structures, respectively), the α-helix, the loop containing residues from Y96 to F105 (colored in red and blue, respectively in the trans and cis structures) and the β-strand (colored in pale yellow and magenta, respectively) b) In the cis conformation, the Leu76-Lys77 peptide bond interacts across the dimer interface with Nξ establishing a hydrogen bond with the backbone carbonyl of Glu 108 in the above mentioned β-strand of the neighboring subunit. Another cross-talk across the dimer interface involves a salt-bridge between Arg 80 and Glu108 of A and B subunits. The figure has been generated using Pymol.

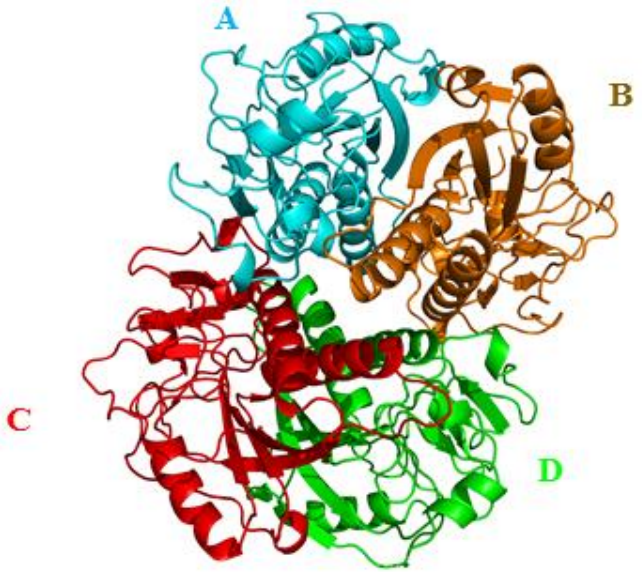

Figure S20. PfHGXPRT tetramer with the subunits A (cyan), B (brown), C (red) and D (green). The tetramer is the catalytically active form of the enzyme.[S2] Isomerization of Leu76-Lys77 peptide bond and tetramerization of PfHGXPRT would establish additional cross-talk between subunits A and B and also between subunits A and D. The tetramer has been generated from PfHGXPRT structure (1CJB) using PISA server.[S8]

Table S1. Kinetic parameters of PfHGXPRT mutants F197W and W181S/F197W[a]

KINETIC PARAMETERS	SUBSTRATE	ENZYME	UNACTIVATED	IMP ACTIVATED
K_m (μM)	Xanthine	F197W	31±4	22±4
		W181S/F197W	5±1	10±2
	PRPP.Mg^{2+}	F197W	641±90	212±25
		W181S/F197W	2064±525	544±112
k_{cat} (sec^{-1})	Xanthine	F197W	0.2	0.9
		W181S/F197W	0.04	0.8
	PRPP.Mg^{2+}	F197W	0.2	1.6
		W181S/F197W	0.04	0.8

[a]Activation of tryptophan mutants was carried out by the same procedure as mentioned for PfHGXPRT. In order to estimate the K_m for PRPP for unactivated and IMP activated F197W, the substrate concentration was varied from 0.1 mM

– 5 mM and 0.025 mM – 2 mM, respectively. Xanthine concentration was maintained at 100 μM in both cases. For estimation of K_m for xanthine, it was varied from 5 μM – 200 μM with PRPP fixed at 1 mM for both unactivated and IMP activated F197W. In order to estimate the kinetic parameters for unactivated W181S/F197W, PRPP concentration was varied from 1 mM – 7 mM. In case of IMP activated W181S/F197W, PRPP concentration was varied from 0.2 mM - 6 mM. Xanthine concentration was fixed at 50 μM for both unactivated and IMP activated W181S/F197W. K_m for xanthine was estimated by varying it from 2.5 μM – 70 μM in case of unactivated W181S/F197W and from 5 μM – 100 μM in case of IMP activated state. PRPP concentration was fixed at 7 mM and 1 mM, respectively in the unactivated and IMP activated states. Concentration of unactivated F197W or W181S/F197W was fixed at 1 μM and for IMP activated mutants it was fixed at 0.2 μM.

Table S2. Rate constants for association and dissociation of IMP from F197W.IMP complex.

Parameter	Value
K_d **(measured under steady state conditions)**	3.7 μM
k_{on} **(measured from stopped flow spectrophotometer)**	2×10^7 $M^{-1}sec^{-1}$
k_{off} **(measured from stopped flow spectrophotometer)**	9.7 sec^{-1}
K_d **(measured from the ratio** k_{off}/k_{on}**)**	2.1 μM

Movie 1: The movie in .mpeg format shows the opening of catalytic site loop II (red) in PfHGXPRT observed during the unbiased MD simulation of the ligand-free enzyme.

Movie 2: The movie in .mpeg format shows the conformational switch of the Leu76-Lys77 peptide bond and the interaction of the $-NH_3^+$ of the side chain of Lys77 with side chain $-COO^-$ of Glu 144 and backbone carbonyl group of Ile146. This movie is from the WTM simulation, denoted as FES1 in the main manuscript.

References

S1 A. R. Shenoy and S. S. Visweswariah, *Anal. Biochem.*, 2003, **319**, 335–336.

S2 I. Subbayya and H. Balaram, *FEBS Lett.*, 2002, **521**, 72–76.

S3 J. Raman, C. S. Ashok, S. IN Subbayya, R. P. Anand, S. T Selvi and H. Balaram, *FEBS J.*, 2005, **272**, 1900–1911.

S4 M. Frisch, G. Trucks, H. Schlegel, G. Scuseria, M. Robb, J. Cheeseman, G. Scalmani, V. Barone, B., Mennucci, G. Petersson *et al.*, Inc., Wallingford, CT, 2009.

S5 U. Doshi and D. Hamelberg, *J. Phys. Chem. B*, 2009, **113**, 16590–16595.

S6 R. G. Silva and V. L. Schramm, *Biochemistry*, 2011, **50**, 9158–9166.

S7 J. Ko, D. Lee, H. Park, E. A. Coutsias, J. Lee and C. Seok, *Nucleic acids research*, 2011, **352**.

S8 E. Krissinel and K. Henrick, Computational Life Sciences, Springer Berlin Heidelberg, 2005, **3695**, 163–174.